

# GEOLOGICAL NOTE

## Differential Synthetic Aperture Radar Interferometry to Investigate Surface Deformation of the Eastern Snake River Plain, Idaho, U.S.A.

*M. H. Aly, D. W. Rodgers, and G. D. Thackray*

*Department of Geosciences, Idaho State University, Pocatello, Idaho 83209-8072, U.S.A.  
(e-mail: aly@isu.edu)*

### ABSTRACT

The Eastern Snake River Plain (ESRP) is a northeast-trending volcanic basin that marks the track of the Yellowstone hotspot. Subsidence has characterized the ESRP since at least 4 Ma. To test whether subsidence of the ESRP surface is an active process, synthetic aperture radar interferometry has been applied to detect deformation during 1993–2000. Results show that no regionally consistent deformation occurred across the ESRP during the periods of observations. However, local displacements of 1–3-cm magnitude have been detected in the adjacent Basin-Range province. This deformation is not attributed to long-term movement of the ESRP but instead to local tectonic and/or groundwater processes.

### Introduction

The Eastern Snake River Plain (ESRP) is a northeast-trending volcanic basin that marks the path of the Yellowstone hotspot (Morgan 1972; Armstrong et al. 1975). Though standing at a relatively high average elevation of about 1500 m, the ESRP is lower than the surrounding Yellowstone Plateau and Basin-Range province, and several lines of geologic evidence indicate it has experienced significant surface subsidence during the past 4 Ma. Among the lines of evidence are (1) basins and ranges are abruptly downwarped near the ESRP (Kirkham 1931), with as much as 1000 m decrease in surface elevation of ridgelines; (2) the surface elevation of the ESRP diminishes steadily along the track of the hotspot, declining from the Yellowstone Plateau to the southwest; (3) the ESRP and surrounding regions are characterized by axial drainage, wherein tributary streams flow toward the ESRP and its trunk river, the Snake River, which itself flows southwest along the axis of the ESRP; (4) fluvial terraces along the southern ESRP margin are perched 900 m (Late Miocene) and 50 m (early to middle Pleistocene) above the modern ESRP surface (Rodgers et al. 2002); (5) the Big Lost River Trough, a Quaternary fluvio-lacustrine basin within the ESRP, provides evidence of long-lived but localized subsidence within the ESRP (Geslin

et al. 2001); and (6) land surveys indicate centimeter-scale decadal subsidence of the ESRP relative to the Basin-Range province (Reilinger et al. 1977). Regional subsidence at an average rate 5 mm/yr was reported for several traditional leveling profiles (approximately 43–326 km long) across the northeastern part of the ESRP between 1906 and 1967.

Based on these studies, we hypothesized that regional subsidence of the ESRP surface relative to the adjacent Basin-Range province is an active, ongoing process. To test this hypothesis, we conducted a differential synthetic aperture radar interferometry (DInSAR) study that is capable of measuring subcentimeter-scale displacement of the land surface. The objective is to detect and measure the spatial and temporal patterns of surface deformation during 1993–2000 in an area centered on the central ESRP and its adjacent Basin-Range province (fig. 1). This work would advance the understanding of crustal dynamics in the ESRP and its adjacent Basin-Range province and would have an immediate impact on the research of others interested in this area.

### Geologic Setting

The ESRP is approximately 300 km long and 80 km wide, is bounded north and south by the Basin-Range Province, and has no significant faults along

Manuscript received December 24, 2007; accepted September 24, 2008.

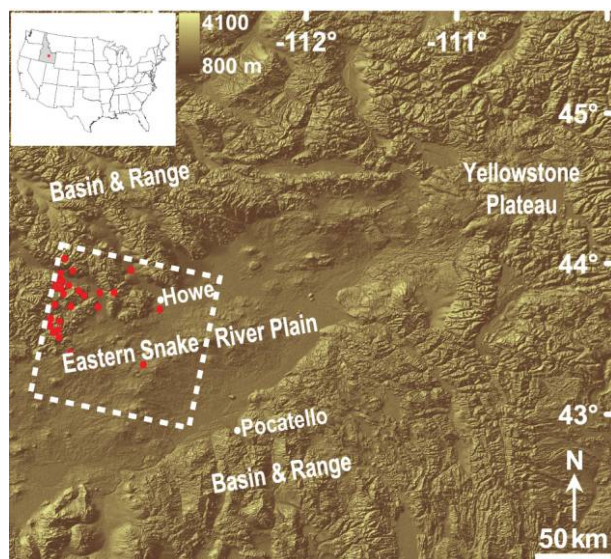


**Figure 1.** Shaded relief image of the Eastern Snake River Plain and its adjacent Basin-Range province. The dotted white box show the coverage of European Radar Satellite data used in this study, and the red dots indicate earthquake locations within that coverage area during the study period from 1993 to 2000 (Suzette Payne, pers. comm., 2007).

its margins (fig. 1). Hotspot-related silicic magmatism occurred on the ESRP from about 10 to 4 Ma, generally progressing to the northeast as North America migrated southwest over the Yellowstone hotspot. Since 4 Ma, the ESRP has been in the wake of the hotspot, and a new pulse of basaltic magmatism has generated a thick layer of lava across the older silicic rocks. Lava and interbedded sediment have accumulated in part because the ESRP is a topographically low region with respect to the surrounding Basin-Range province and Yellowstone plateau. With a surface heat flow less than that at Yellowstone (Blackwell et al. 1992) and a mid-crustal layer more dense than its counterpart in the Basin-Range province (Sparlin et al. 1982), the ESRP is interpreted to be a volcano-sedimentary basin whose subsidence is driven by thermal contraction

(Brott et al. 1981) and/or crustal loading (Anders and Sleep 1992) in the wake of the Yellowstone hotspot.

Just north of the ESRP, mountains and valleys of the Basin-Range province trend north-northwest and plunge south beneath onlapping ESRP volcanic rocks (McQuarrie and Rodgers 1998). West-dipping normal faults cut all rocks and define a half-graben fault pattern. Most range-bounding faults show evidence of Quaternary activity (Pierce and Morgan 1992), and the most active fault scarps coincide with a parabolic zone of recent seismic activity that wraps around the ESRP (Anders et al. 1989). About 60 minor earthquakes (magnitude  $<2.3$ ) occurred in the study area between 1993 and 2000, and their epicenters are almost entirely restricted to the Basin-Range province, as shown in figure 1 (S. Payne, pers. comm., 2007). Vertical movements associated with active Basin-Range faulting may characterize the study area and would be expected to appear as short-term, localized displacements.

### DInSAR Analysis

Fifty-three scenes, spanning 14 yr (1993–2006) and acquired by the European Radar Satellites (ERS-1 and ERS-2), were used to create 34 interferograms for the central part of the ESRP. From the 53 total scenes, five descending-pass scenes spanning 8 yr (1993–2000) were used to create a time-series of four differential interferograms (table 1) using the two-pass interferometric approach. They were then multi-looked, 10 looks in the azimuth direction and two looks in the range direction, to produce interferograms with 40-m dimensions in both azimuth and range directions.

The interferograms were corrected for the flat Earth phase, and the precise baselines were calculated based on the orbital parameters and the average interferogram fringe frequency. The Department of Earth Observation and Space Systems' (Delft University of Technology) precise ERS-1 and -2 state vectors (Scharroo and Visser 1998) were used to compensate for orbital inaccuracies. Elevation data of 1 arc second from the Shuttle Radar

**Table 1.** European Radar Satellite Raw Data Used in This Study

| Track | Frame | Reference image |         |          | Slave image |         |          | $B_{\perp}$ | $\sigma$ |
|-------|-------|-----------------|---------|----------|-------------|---------|----------|-------------|----------|
|       |       | Orbit           | Mission | Date     | Orbit       | Mission | Date     |             |          |
| 356   | 2727  | 07224           | ERS-2   | 06091996 | 10020       | ERS-1   | 15061993 | .2          | .001     |
|       |       | 16242           | ERS-2   | 29051998 | 06222       | ERS-2   | 28061996 | 17          | .079     |
|       |       | 28767           | ERS-2   | 20102000 | 16242       | ERS-2   | 29051998 | 42          | .196     |
|       |       | 28767           | ERS-2   | 20102000 | 06222       | ERS-2   | 28061996 | 25          | .117     |

Note. Date is day, month, year.  $B_{\perp}$  is the perpendicular baseline (in meters);  $\sigma$  is the phase error (in radians) caused by the topographic uncertainty of the Shuttle Radar Topography Mission digital elevation model.

Topography Mission (SRTM) were used to correct the interferometric phase for topography, and the interferograms produced were then filtered using the nonlinear adaptive filter developed by Goldstein and Werner (1998) to reduce the amount of phase noise. The atmospheric phase is uncorrelated temporally and is of low frequency spatially (Zebker et al. 1997); thus, the degree to which atmospheric artifacts were present in a specific SAR acquisition

could be assessed by a pairwise comparison of interferograms (Massonnet and Feigl 1995). The differential interferometric phase was unwrapped using the minimum cost-network flow algorithm developed by Costantini (1998), and the unwrapped phase values were converted later into line-of-sight (LOS) deformation (mm; fig. 2).

Phase errors ( $\sigma$ ) caused by the 7-m topographic uncertainty of SRTM digital elevation model (DEM;

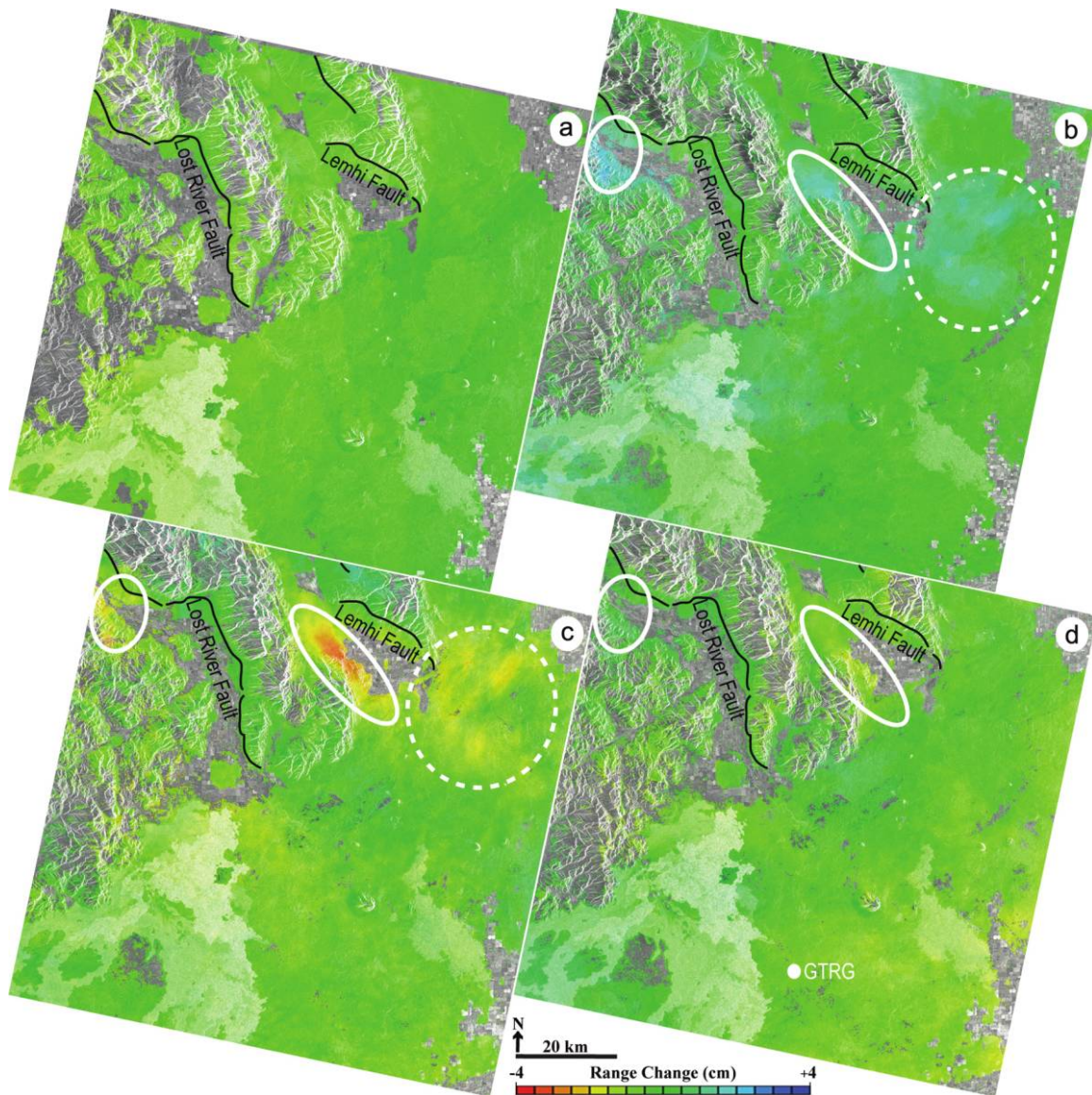


**Figure 2.** Line-of-sight surface deformation during 1993–2000, superimposed on the reference intensity image of each pair: *a*, from June 15, 1993, to September 6, 1996; *b*, from June 28, 1996, to May 29, 1998; *c*, from May 29, 1998, to October 20, 2000; and *d*, from June 28, 1996, to October 20, 2000. The solid white ovals denote the most likely deformation features, and the dotted white circles mark suspected areas of either deformation or atmospheric artifacts. The solid black lines indicate major faults in the study area, and the white dot in *d* indicates the location of the Great Rift global positioning system station.

estimated by Farr and Kobrick [2000]) were calculated for each ERS interferogram and are provided in table 1. The short perpendicular baselines ( $<50$  m) of ERS pairs used in this study and the error in SRTM DEM might lead to a phase error up to 0.196 rad, which is below the typical phase noise level of ERS-1 and ERS-2, on the order of about 0.70 rad (Hanssen 2001). Thus, the topographic contribution to the phase error is negligible.

The altitude-dependent atmospheric phase delay was calculated using linear regression and subtracted from the corrected, unwrapped phase. Because of the lateral topographic variability in the study area, this process was limited to areas of rough topography ( $>2000$  m) using a Boolean mask. The effectiveness of this approach was tested using a tandem ERS interferogram to make sure that the signal from real deformation was not partially removed.

### Results

Of the 34 ERS interferograms that were processed for the study area, four representative interferograms were selected to demonstrate a time series of surface displacement between 1993 and 2000. Three interferograms (1996–1998, 1998–2000, 1996–2000) were selected because they are the only ones to show localized regions of consistent deformation, that is, deformation that can be tracked in the same location in a time series of differential interferograms. The selected interferograms were used to generate four surface deformation maps (fig. 2) showing LOS surface movements over a large area (approximately 10,000 km<sup>2</sup>) that includes the central ESRP and its adjacent Basin-Range province. The minimum value of observed LOS surface movement is about  $-3$  cm, and the maximum value is about  $+2$  cm.

Across the ESRP, all surface displacement maps (fig. 2) show that no LOS, regionally consistent deformation occurred in excess of the calculated upper-bound phase error (0.9 mm). The slight variations in color over the ESRP (including the area surrounded by the dashed white circle) are most likely related to imperfect removal of atmospheric artifacts rather than real surface deformation, as they are not consistent over time with independent interferograms. These results indicate either that the ESRP surface moved less than the upper-bound phase error (0.9 mm) that could be masked by seasonal changes in groundwater levels or that the ESRP surface might not have moved at all during the periods of observations. This observation was witnessed in every one of the 34 interferograms

processed for this study, providing conclusive evidence of the lack of LOS displacement during 1993–2006.

Across the Basin-Range province, vertical surface movements of limited regional extent have been detected in restricted locations (fig. 2*b–2d*). These movements are shown in a time series of LOS surface deformation maps, evidence that they may represent real surface deformation. The elongated feature northwest of Howe is present in figure 2*b–2d*, which means the deformation is associated with at least the acquisitions dated May 29, 1998, and October 20, 2000. The deformation pattern is not believed to be associated with the acquisition dated June 28, 1996 because the 1993–1996 interferogram (fig. 2*a*) does not show a similar pattern.

### Discussion

DInSAR results do not support the hypothesis that the ESRP is actively subsiding relative to the adjacent Basin-Range province. Despite several lines of geologic evidence for long-term ( $>1$  m.yr.) subsidence, no short-term (2–8 yr) subsidence is detected in any of the 34 interferograms analyzed for this study. Surface changes marked with the dotted white circles (fig. 2*b, 2c*) are not observed in independent interferograms; thus, they are suspected to be atmospheric effects associated with the ERS acquisition dated May 29, 1998, rather than real surface deformation. The absence of ESRP surface displacement is independently supported by continuous measurements at the Great Rift global positioning system (GPS) station (fig. 3), which indicate no consistent vertical deformation occurred during the 1999–2006 period ([http://www.uusatrg.utah.edu/Site\\_Info/gtrg.html](http://www.uusatrg.utah.edu/Site_Info/gtrg.html)). As no re-

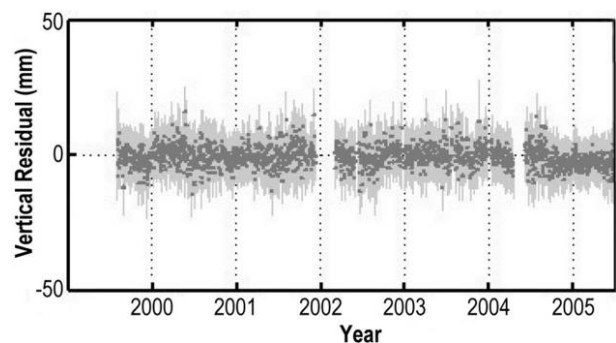


**Figure 3.** Time series of the Great Rift global positioning system (GTRG GPS) station ([http://www.uusatrg.utah.edu/Site\\_Info/gtrg.html](http://www.uusatrg.utah.edu/Site_Info/gtrg.html)). Location of the GTRG GPS station is shown in figure 2*d*.

gional subsidence is detected by geodetic measurements (DInSAR and GPS) across the ESRP during 1993–2006, the short-term subsidence in the eastern ESRP (about 75 km east of our study area) that was observed with leveling surveys between 1906 and 1967 by Reilinger et al. (1977) appears to be related to a nonlinear, local event that is not currently affecting the ESRP.

Short-term active subsidence of  $<0.3$  mm/yr across the central ESRP is, however, still permitted by the geodetic data, since displacements at this rate fall in the limit of phase error of both DInSAR and GPS measurements over time spans of 2–8 yr. The cumulative effect of such a slow rate of subsidence could be masked by oscillations in the groundwater levels over short time spans, but if this slow rate of subsidence were occurring over  $10^6$  yr, the cumulative effect would be significant. In fact, average surface subsidence rates based on geologic data are similarly slow: using the elevation of Late Miocene (about 7 Ma) strath terraces near Pocatello (fig. 1) as a proxy for the former ESRP elevation, the average ESRP subsidence rate would be 0.13 mm/yr, while assuming the central ESRP was once at the same elevation as modern Yellowstone Plateau yields an average subsidence rate of about 0.1 mm/yr. These rates disregard the effects of emplacing approximately 1000 m of Pliocene and Pleistocene basalt onto the central ESRP, but isostatic compensation would yield a net elevation increase of only 15%–20% of the cumulative basalt thickness (McQuarrie and Rodgers 1998). Actually, if ESRP long-term surface subsidence rates did exceed 0.3 mm/yr since 7 Ma, the result would be a basin whose elevation would be  $>2$  km below the adjacent Basin-Range province or a basin filled with  $>5$  km of post-hotspot basalt and sediment. Neither of these options describes the modern ESRP. Thus, the results of this DInSAR analysis are exactly what should be expected: no evidence of regionally extensive surface displacement in excess of 0.3 mm/yr.

Areas of local deformation marked with solid white ovals (fig. 2*b–2d*) are coincident with seismic activity (fig. 1) in the Basin-Range province during the same approximate time span, implying that surface deformation is related to slight movements along normal faults. One deformation feature is located in the hanging wall of the Lost River normal fault, but the other one that is located northwest of Howe (fig. 1) does not coincide with any of the Quaternary active faults that were obtained from the USGS database. The northwest orientation of the deformation feature northwest of Howe is parallel to the dominant strike of nearby active normal

faults in the Basin-Range province. Our preferred interpretation is that displacement reflects minor slip along an underlying blind normal fault. However, the large magnitude of surface change apparent in figure 2*b–2c* might be partially influenced by atmospheric artifacts associated with the ERS acquisition dated May 29, 1998. Ancillary atmospheric data are needed to quantify and remove atmospheric artifacts accurately but are not available for this study.

The study area is a closed basin, wherein all surface water from rains and melted snow flow directly to the aquifer system. In addition, intensive agricultural production (marked by the interferometric phase decorrelation in fig. 2) is frequently dependent on groundwater withdrawal for irrigation. The elongated feature northwest of Howe is located at the intersection of the Little Lost River and an inactive normal fault (not shown in fig. 2). Therefore, the groundwater recharge/discharge also might have a role in the detected local surface movements and this could interpret the inversed interferometric signals in the differential interferograms. We cannot test this hypothesis because no records of groundwater pumping or recharge are kept for the study area, nor are there any records of local precipitation.

## Conclusions

No regionally consistent surface subsidence or uplift was detected across the central ESRP during 1993–2000. Either the ESRP was not active, or it deformed at a rate slower than the upper-bound phase error (0.9 mm) during the periods of ERS observations. Localized deformation apparently related to tectonic and/or groundwater processes has been detected in the Basin-Range province immediately adjacent to the northwestern edge of the ESRP, where earthquake activities are documented. These local events are characterized by nonlinear surface displacements over short time periods.

## ACKNOWLEDGMENTS

This study is funded by NASA Experimental Project to Stimulate Competitive Research grant NCC5-577 to Idaho State University. J. Chadwick completed a preliminary analysis of synthetic aperture radar data under the auspices of this grant. European Radar Satellite data are provided at the production cost by the European Space Agency under Category 1 Proposal 4242. The seismic data and locations of the major fault segments in the study area were provided by Suzette Payne of the Idaho

National Laboratory. Shuttle Radar Topography Mission digital elevation model data were obtained from the NASA JPL. We appreciate reviews by the

editor and two anonymous reviewers, whose constructive comments significantly improved the manuscript.

---

#### REFERENCES CITED

- Anders, M. H.; Geissman, J. W.; Piety, L. A.; and Sullivan, J. T. 1989. Parabolic distribution of circum-eastern Snake River Plain seismicity and latest Quaternary faulting: migratory pattern and association with the Yellowstone hotspot. *J. Geophys. Res.* 94:1589–1621.
- Anders, M. H., and Sleep, N. H. 1992. Magmatism and extension: the thermal and mechanical effects of the Yellowstone hotspot. *J. Geophys. Res.* 97: 15,379–15,394.
- Armstrong, R. L.; Leeman, W. P.; and Malde, H. E. 1975. K-Ar dating, Quaternary and Neogene volcanic rocks of the Snake River Plain, Idaho. *Am. J. Sci.* 275: 225–251.
- Blackwell, D. D.; Kelley, S.; and Steele, J. L. 1992. Heat flow modeling of the Snake River Plain, Idaho. Contract report DE-AC07-761DO1570. Washington, DC, U.S. Department of Energy, 109 p.
- Brott, C. A.; Blackwell, D. D.; and Ziagos, J. P. 1981. Thermal and tectonic implications of heat flow in the eastern SRP, Idaho. *J. Geophys. Res.* 86:709–734.
- Costantini, M. 1998. A novel phase unwrapping method based on network programming. *IEEE Trans. Geosci. Remote Sens.* 36:813–821.
- Farr, T. G., and Kobrick, M. 2000. Shuttle Radar Topography Mission products as a wealth of data. *EOS: Trans. Am Geophys. Union* 81:583–585.
- Geslin, J. K.; Link, P. K.; Riesterer, J. W.; Kuntz, M. A.; and Fanning, C. M. 2001. Pliocene and Quaternary stratigraphic architecture and drainage systems of the Big Lost Trough, northeastern Snake River Plain, Idaho. *In* Link, P. K., and Mink, L. L., eds. *Geology, hydrogeology, and environmental remediation, Idaho National Engineering and Environmental Laboratory, Eastern Snake River Plain, Idaho.* *Geol. Soc. Am. Spec. Pap.* 353:11–27.
- Goldstein, R., and Werner, C. 1998. Radar interferogram filtering for geophysical applications. *Geophys. Res. Lett.* 25:4035–4038.
- Hanssen, R. 2001. Radar interferometry: data interpretation and error analysis. Boston, Kluwer Academic, 308 p.
- Kirkham, V. R. D. 1931. Snake River downwarp. *J. Geol.* 39:456–487.
- Massonnet, D., and Feigl, K. 1995. Discrimination of geophysical phenomena in satellite radar interferograms. *Geophys. Res. Lett.* 22:1537–1540.
- McQuarrie, N., and Rodgers, D. W. 1998. Subsidence of a volcanic basin by flexure and lower crustal flow: the eastern Snake River Plain, Idaho. *Tectonics* 17: 203–220.
- Morgan, W. J. 1972. Plate motions and deep mantle convection. *Geol. Soc. Am. Mem.* 132:7–22.
- Pierce, K. L., and Morgan, L. A. 1992. The track of the Yellowstone hotspot: volcanism, faulting and uplift. *In* Link, P. K.; Kuntz, M. A.; and Platt, L. B., eds. *Regional geology of eastern Idaho and western Wyoming.* *Geol. Soc. Am. Mem.* 179:1–53.
- Reilinger, R. E.; Citron, G. P.; and Brown, L. D. 1977. Recent vertical crustal movements from precise leveling data in southwestern Montana, western Yellowstone National Park and the Snake River Plain. *J. Geophys. Res.* 82:5349–5359.
- Rodgers, D. W.; Ore, H. T.; Bobo, R.; McQuarrie, N.; and Zentner, N. 2002. Extension and subsidence of the eastern Snake River Plain. *In* Bonnichsen, B.; White, C.; and McCurry, M. O., *Tectonic and magmatic evolution of the Snake River Plain volcanic province.* *Idaho Geol. Surv. Bull.* 30:121–160.
- Scharroo, R., and Visser, P. 1998. Precise orbit determination and gravity field improvement for the ERS satellites. *J. Geophys. Res.* 103:8113–8127.
- Sparlin, M. A.; Braile, L. W.; and Smith, R. B. 1982. Crustal structure of the eastern Snake River Plain determined from ray trace modeling of seismic refraction data. *J. Geophys. Res.* 87:2619–2633.
- Zebker, H.; Rosen, P.; and Hensley, S. 1997. Atmospheric effects in interferometric synthetic aperture radar surface deformation and topographic maps. *J. Geophys. Res.* 102:7547–7563.